OPTIMIZATION AND ANALYSIS OF AERODYNAMIC CHARACTERISTICS AND NOISE SOURCE IN A CENTRIFUGAL COMPRESSOR WITH VANED DIFFUSER

Huabing WEN[1], Jingjing SANG[2], Qidong ZHONG[3], Hongdan LIU[4]

In this paper the turbulence dynamics and the noise source of a centrifugal turbocharger compressor were analyzed using Computational Fluid Dynamics (CFD) techniques. The effects of the diffuser radius and the inlet angle of vane leading edge on the aerodynamic performance were also researched. In order to increase the static pressure recovery coefficient and reduce the total pressure loss coefficient, one kind optimized diffuser was developed. The results show that: The static pressure recovery coefficient and the total pressure loss coefficient increase gradually in the radial direction. The regions of the separate flows, the secondary flows and the wake flows are the main noise sources in diffuser; the shedding of thick boundary layer and the vortex motion result in the high-level noise.

Keywords: centrifugal compressor, aerodynamic characteristic, noise source, CFD, vaned diffuser

1. Introduction

Centrifugal compressor, as one important part of the turbocharger, has been widely used in transportation and power stations. With the ever-growing demands for small dimension and high performance, the aerodynamic analysis and the performance optimization become more and more essential. A centrifugal can be divided into three parts: the impeller, the diffuser and the volute. The rotating impeller transfers a large amount of energy to the fluid. Even for better diffusion, at the improved-design impeller outlet, more than 50 % of the transferred energy still remains available as kinetic energy. This energy is then converted into static pressure in the stationary diffuser, which, however, is responsible for at least 1/3 of the overall fluid dynamic losses occurring in a centrifugal compressor, therefore the diffusers have a great effect on the compressors.

[1] Institute of Noise and Vibration, Jiangsu University of Science and Technology, China, email: wen-huabing@163.com
[2] Institute of Noise and Vibration, Jiangsu University of Science and Technology, China, email: sjjjust@163.com
[3] Institute of Noise and Vibration, Jiangsu University of Science and Technology, China
[4] Chongqing Jiangjin Shipbuilding Industry CO.,LTD, China

Although a lot of research has been done on the volute and impeller, there are very few detailed studies dealing with the performances of the diffusers in [2-3].TAN Wei et al. [4] designed one kind adjustable diffuser, and found that the adjustment of diffusers played an important role in improving the performance and reducing the head losses. As the vanes leading to the narrow operating range and large incidence losses, Du Jian-Yi et al. [5] made an intensive investigation on the influence of the vane shape and incidence angle on the flow in the diffusers. Engeda A [6] studied the effect of the solidity on the performance of diffusers, and developed numerical simulation methods for analyzing and predicting the performance and noise of the centrifugal compressor. Sun H also optimized the impeller geometry in [3,7]. Ohta Y et al. [8] performed experiments on a centrifugal compressor to investigate the influence of the shape of the diffuser vane leading edge on the aerodynamic noise, and they designed a kind of vanes to reduce the noise of centrifugal compressor. Wen H B discussed the noise generation mechanism of the marine diesel engine turbocharger, and carried out the experiments to study the dominant noise source by the spectrum analysis and sound intensity identification technique[9]. In this paper, our goal was (1) optimizing the incidence angle and the shape of the leading edge of the vanes with multi-scheme, and (2) by comparing the flow fields and the flow noise in different design schemes, analyzing the influence of them on the performance of the compressor.

2. Research object and numerical method

2.1 Research object

We consider a marine turbocharger compressor, with the design rotating speed of 28200 *r/min* and a volume flowrate of $3.75\,m^3/s$ at design point, consisting of 10 impeller blades and 10 splitters. Inside the diffuser with radius of r, and the incidence angle of θ, there are 19 airfoil vanes with round head. Geometry of the impeller and diffuser is illustrated in Fig. 1 .

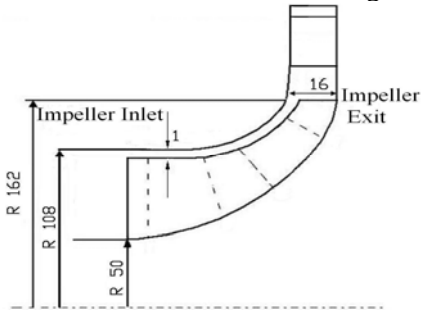

Fig.1. Main dimensions (in mm) of impeller and diffuser

The incidence angle of the diffuser vanes θ range from 15°to 25, given by:

$$\theta = \theta_3 + (2^\circ \sim 5^\circ) \tag{1}$$

where θ_3 is the flow angle. According to the experimental study performed by the Soviets, when $\theta = 22^\circ \sim 24^\circ$, the best performance of compressor can be acquired[10]. Therefore, the incidence angle of the vanes will be fine adjusted to select the optimized design scheme, and nine design schemes are given in Tab. 1.

Table 1

Optimization scheme

Schemes: Radius / Angle	r	3r	r/3
θ	1	4	7
$\theta - 3^\circ$	2	5	8
$\theta + 2^\circ$	3	6	9

2.2 Numerical method

2.2.1 Numerical model and meshing

Flow at the diffuser inlet, which affects the diffuser performance, is 3D non-uniform turbulent. Diffuser inlet flow conditions are affected by the flow leaving the impeller, whose velocity usually varies due to recirculation and separation in the impeller. For the high pressure ratios, the tangential velocity will be very high at the impeller exit, and the flow may be locally supersonic at the diffuser inlet, causing shock waves and boundary layer separation. These phenomena will lead to the strong interference between the impeller and diffuser, and will impact on the diffuser performance [11]. As a consequence, in order to study the flow and analyze the formation mechanism of the noise source, the optimization work has been performed in a numerical domain which includes both the impeller and vaned diffuser. To accommodate the complexity of the compressor structure, and to improve the mesh quality, the multiblock grid and unstructured grid are used for the discrete model. The relatively fine grids of about 327,000 elements have been generated for the impeller to analyze the flow accurately, and 91,000 elements applied in the inlet pipe. The number of grids for diffusers in different schemes is basically identical, about 50,000 elements. Fig. 2 shows the boundaries definition of the nineteenth computational domain.

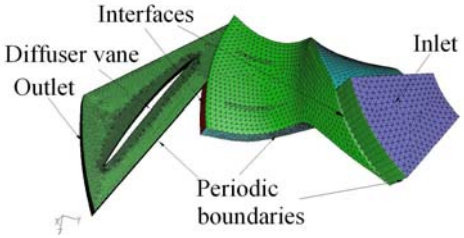

Fig.2 Grids of the computational domain

The governing equations are 3D, steady, compressible Navier–Stokes equations and can be given in conservation law form by

$$\frac{\partial}{\partial x_i}(\rho u_i) = 0 \tag{2}$$

$$\begin{aligned}\frac{\partial}{\partial x_j}(\rho u_i u_j) = &-\frac{\partial p}{\partial x_i} + \frac{\partial}{\partial x_j}\left[\mu\left(\frac{\partial u_i}{\partial x_j} + \frac{\partial u_j}{\partial x_i} - \frac{2}{3}\delta_{ij}\frac{\partial u_k}{\partial x_k}\right)\right] \\ &+ \frac{\partial}{\partial x_j}\left[\mu_t\left(\frac{\partial u_i}{\partial x_j} + \frac{\partial u_j}{\partial x_i}\right) - \frac{2}{3}\delta_{ij}\left(\mu_t\frac{\partial u_k}{\partial x_k} + \rho k\right)\right]\end{aligned} \tag{3}$$

$$\frac{\partial}{\partial x_i}\left[u_i(\rho E + p)\right] = \frac{\partial}{\partial x_i}\left[k_{eff}\frac{\partial T}{\partial x_i} - \sum_{j'} h_{j'} J_{j'} + u_j\left(\tau_{ij}\right)_{eff}\right] + S_h \tag{4}$$

where, ρ, u, p μ, and μ_t represent density (kg/m3), velocity (m/s), pressure (Pa), dynamic viscosity ($\mathrm{Pa\cdot s}$) and turbulent viscosity ($\mathrm{Pa\cdot s}$) of the air respectively. k represents the turbulence kinetic energy ($\mathrm{m^2/s^2}$). The subscripts i, j, and k represent the directions (x, y, z). δ_{ij} represents the Kronecker delta, with $\delta_{ii} = 1$, and $\delta_{ij} = 0, i \neq j$. T is the temperature (K), E is the total energy (divided by mass) ($\mathrm{kJ/kg}$), $E = h - \frac{p}{\rho} + \frac{u^2_i}{2}$, h represents the enthalpy ($\mathrm{kJ/kg}$). And the effective thermal conductivity k_{eff} is given by:

$$k_{eff} = k + \frac{c_p \mu_t}{\mathrm{Pr}_t} \tag{5}$$

where, k is the thermal conductivity of air ($\mathrm{W/(m\cdot K)}$), and c_p is the specific heat capacity of air ($\mathrm{J/(kg\cdot K)}$), $J_{j'}$ is the diffusion flux of species j, includes the heat of chemical reaction, and any other defined volumetric heat sources. A constant value of 0.85 is used for the turbulent Prandtl number Pr_t. And the term $(\tau_{ij})_{eff}$ is the viscous heating ($\mathrm{kg/(m\cdot s^2)}$).

In [12], the results indicate that the RNG k-epsilon model overall yields better results than the standard k-epsilon and RSM models. So turbulence in this paper is also simulated with the RNG k-epsilon model. The conservation equations for the turbulent kinetic energy k and its rate of dissipation ε are given by:

$$\frac{\partial}{\partial t}(\rho k)+\frac{\partial}{\partial x_i}(\rho k u_i)=\frac{\partial}{\partial x_j}\left[\alpha_k \mu_{eff}\frac{\partial k}{\partial x_j}\right]+G_k+G_b-\rho\varepsilon-Y_M+S_k \tag{6}$$

$$\frac{\partial}{\partial t}(\rho \varepsilon)+\frac{\partial}{\partial x_i}(\rho \varepsilon u_i)=\frac{\partial}{\partial x_j}\left[\alpha_\varepsilon \mu_{eff}\frac{\partial \varepsilon}{\partial x_j}\right]+\frac{C_{1\varepsilon}\varepsilon}{k}(G_k+C_{3\varepsilon}G_b)-C_{2\varepsilon}\rho\frac{\varepsilon^2}{k}-R_\varepsilon+S_\varepsilon \tag{7}$$

where α_k and α_ε are the inverse effective Prandtl numbers for k and ε respectively. G_k ($\mathrm{kg/(m\cdot s^3)}$) represents the generation of turbulence kinetic energy due to the mean velocity gradients. G_b ($\mathrm{kg/(m\cdot s^3)}$) is the generation of turbulence kinetic energy due to buoyancy. Y_M ($\mathrm{kg/(m\cdot s^3)}$) represents the contribution of the fluctuating dilatation in compressible turbulence to the overall dissipation rate. The model constants $C_{1\varepsilon}$, $C_{2\varepsilon}$ and $C_{3\varepsilon}$ in Equation (7) are valued by the RNG theory, with $C_{1\varepsilon}=1.42$, $C_{2\varepsilon}=1.68$, $C_{3\varepsilon}$ =1.0, by default in FLUENT. S_k and S_ε are user-defined source terms respectively.

2.2.2 Boundary conditions

According to the physical meaning for turbomachinery flow simulations, the modelled boundary conditions can be defined as: (1) At the inlet, we consider that the inlet velocity (96.7m/s, 108.3m/s, 115.0m/s, 125.0m/s, 131.7m/s) is uniform in each grid node, the flow direction is perpendicular to the inlet surface, and the turbulence intensity is 5%, so that the total pressure and temperature can be specified as 1.01E5 Pa and 300 K respectively. (2) At outlet of the computational domain, the total pressure is also defined. (3) The lateral faces of the domain have been specified as rotational periodic boundaries, and (4) the walls have been modeled as adiabatic by using standard wall functions, thus all of the wall boundary conditions in the volute and impeller are regarded as no-slip conditions.

For the steady-state simulations, a mixing plane approach has been used at the interface between the rotating impeller and the stationary diffuser to simulate the interference accurately. The working fluid is ideal gas. The discrete equations are solved by using the implicit separation method. The pressure – velocity coupling is calculated through the SIMPLEC algorithm. Third order, QUICK scheme is used for convection terms and second order central difference schemes

for diffusion terms. The convergence condition of the simulation is that the unbalanced error of the mass, momentum and energy in the computational domain reduced to the value of 0.1%.

3. Analysis of flow field and sound field

3.1. Analysis of the flow field

The optimization of the compressor is mainly based on the improvement of the structure of diffuser, therefore, the aerodynamic performance analysis of the compressor is concentrated on the flow in different diffusers.

The pressure ratio of diffusers in different schemes is illustrated in Fig. 3. As can be seen from it, the pressure ratios in scheme 7 and 9 are higher than others. Besides, the pressure ratios in other optimized designs are lower than prototype machine (scheme 1).

The pressure ratio (π_c) of the compressor is calculated based on the total pressures (p_{total}, in Pa) at both the inlet and outlet of the model, as defined below:

$$\pi_c = \frac{p_{total,outlet}}{p_{total,inlet}} \tag{8}$$

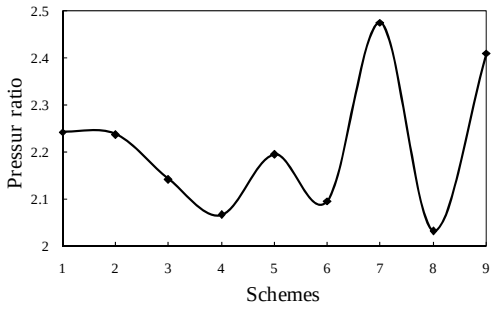

Fig.3 Pressure ratios in different schemes

Fig. 4 shows the distribution of the circumferentially-averaged total pressure in radial direction. The distributions of total pressure in schemes are different, which present the downward trend in the radial and prove that much large head losses appear at exit. The total pressure in scheme 1 and 2 decrease reposefully, while the scheme 7 and 9 hold relatively high level, leading to the corresponding high pressure ratio, this is identical with Fig. 3. As the diffuser vane leading edges are located at the radius ranging from 0.175~0.185m, impacted by the high speed airflow from the impeller exit, resulting in the great head losses, the sudden drawdown of total pressure ocours from scheme 3 to 7. The flow condition will cause larger pressure difference between the pressure side and the suction side, which also leads to the drop of the aerodynamic performance of compressor and

the increase of the flow noise. Therefore, the inlet angle or the radius of diffuser vane leading edges in scheme from 3~7 dismatch with the flow at the impeller exit, which need to be adjusted. In scheme 4~6 sudden drawdown of the total pressure appears at the diffuser vane inlet and the values are very low at the diffuser exit, relevant analysis shows the round head radius of the diffuser vane leading edge is one of the main reasons of head losses. So, in order to make the flow at the diffuser inlet more smoothly, the round head radius should be minimized in the design process of the diffuser vane.

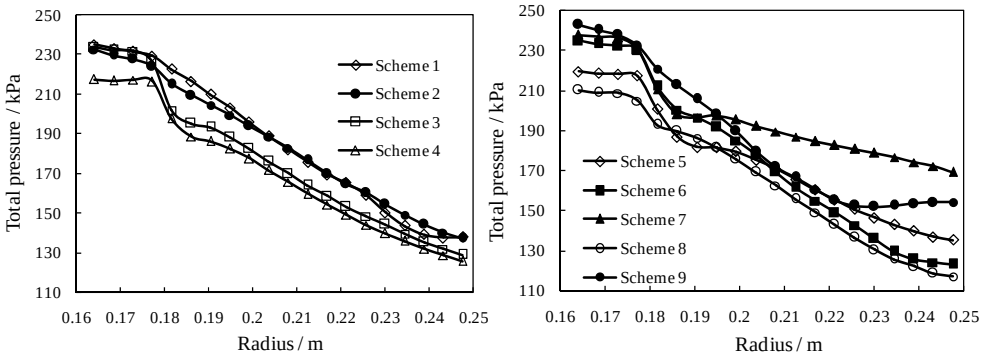

Fig.4 Distribution of total pressure in radial direction

Taking the velocity vector at the mid-span of the diffuser in scheme 6 for instance, as illustrated in Fig.5, the results show that supersonic flow appears at the vane leading edge, and the impact occurs on the pressure side. It leads to the decrease of the speed on suction side, the vortex motion appearing in large range on the suction side of the blade tail, and the head losses increasing. The flow speed is much lower on the suction side of diffuser vane, where the inverse flow and the separation of the boundary layer were caused by the severe turbulence flow. The flow condition has an important effect on the scale of the aerodynamic noise source. The similar flow conditions can also be observed in scheme from 2~8, therefore, following research will be focused on analyzing scheme 1 and 9.

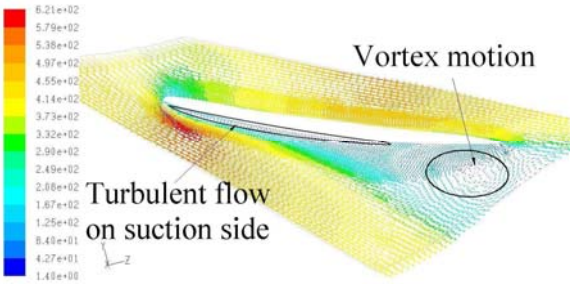

Fig.5 Velocity vector at the mid-span of the diffuser in scheme 6(unit: m/s)

Fig. 6 shows the contour maps of Mach number in scheme 1 and 9. A supersonic Mach number is visible, which exhibits a shock on the vane pressure side, very close to the leading edge. With the development of flow, the velocity decreases gradually. The boundary layer is much thick on the vane suction side, and higher speed is found on the pressure side. In scheme 1, low speed vortex motion appears at the vane trailing edge, the flow in scheme 9 is smoother, without separated vortex, which is better than flow in scheme 1. From Fig. 7, the causes of the vortex on suction side can be concluded, for the absolute values of the air inlet angle in scheme 1 are wholly lower than in scheme 9, therefore, the air inlet angle in scheme 1 is too large, which leads to the impact between the airflow and the vane leading edge.

To compare the flow results in different schemes, two important parameters are used to evaluate the performance of a diffuser: the static pressure recovery coefficient (C_p) and the total pressure loss coefficient (φ), given by:

$$C_p = (p - \overline{p}_3) / (\overline{p}_{03} - \overline{p}_3) \tag{9}$$

$$\varphi = (\overline{p}_3 - p_0) / (\overline{p}_{03} - \overline{p}_3) \tag{10}$$

Where, $\overline{p}_3$ and $\overline{p}_{03}$ indicate the averaged static pressure and the averaged total pressure of the diffuser exit respectively, while p and p_0 stand for the static pressure and the total pressure of the diffuser respectively.

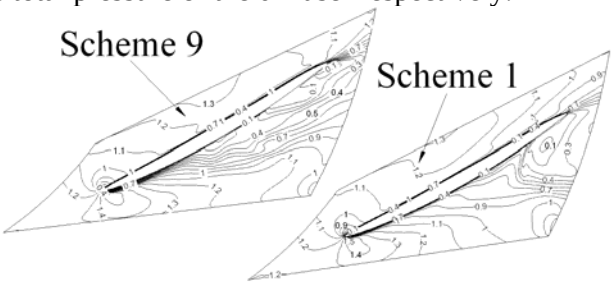

Fig.6 Distribution of Mach number in scheme 1and scheme 9

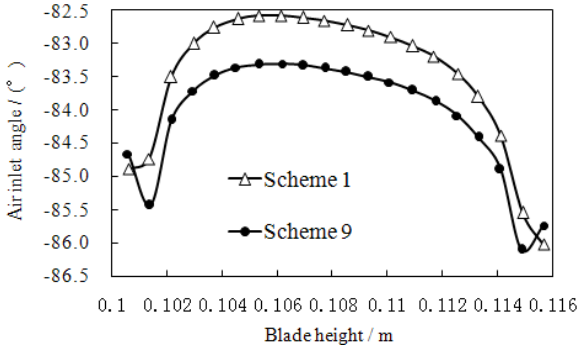

Fig.7 Flow angles along blade height at diffuser inlet

Fig. 8 shows the distribution of the circumferentially-averaged static pressure recovery coefficient in radial direction at mid-span in scheme 1 and scheme 9. The overall level of C_p in diffuser in scheme 9 is higher than in scheme 1. Because of the high velocity and the lower average static pressure than diffuser exit, C_p is less than zero at some parts of diffuser in scheme 1. The inlet angle of vane leading edge and the radius of round head in scheme 9 are more appropriate for the increase of C_p in diffuser.

The distribution of the circumferentially-averaged total pressure loss coefficient (φ)in radial direction at mid-span Fig. 9 is illustrated in scheme 1 and 9. Where, φ increases in the flow direction, and the maximum value can be obtained at diffuser exit. The overall level of φ in diffuser in scheme 1 is higher than in scheme 9. Therefore, taking φ and C_p as the evaluating indexes to evaluate the performance of diffuser, scheme 9 is much better than scheme 1 to match with the compressor.

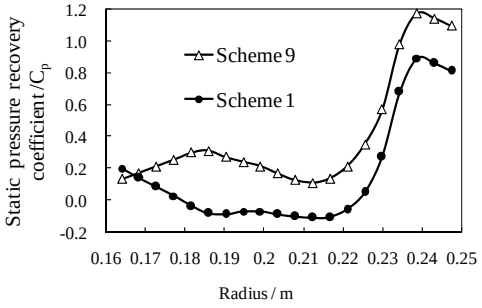

Fig.8 Distribution of C_p in radial direction at mid-span

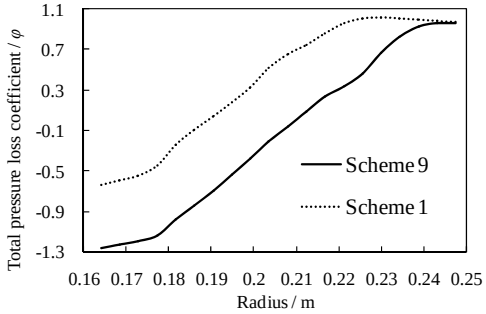

Fig.9 Distribution of φ in radial direction at mid-span

3.2 Analysis of sound field

Due to the complexity of flow characteristics, and severe turbulent flow in large range of diffuser, the noise usually have no distinct tones, thus the sound energy is continuously distributed over a broad range of frequencies [13-14]. Consequently, the broadband noise model can be utilized to analyze the overall distribution characteristics of the near-field noise source in compressor, in conjunction with Proudman's formula, a formula for acoustic power generated by isotropic turbulence without mean flow.

$$P_A = \alpha\rho_0(\frac{u^3}{l})\frac{u^5}{a_0^5} \tag{11}$$

where α is a model constant, u and l are the turbulence velocity and length scales, respectively, and a_0 is the speed of sound. In terms of k and ε, Equation (11) can be rewritten as

$$P_A = \alpha_\varepsilon \rho_0 \varepsilon M_t^5 \tag{12}$$

where, $M_t = \frac{\sqrt{2k}}{a_0}$, the rescaled constant α_ε is set to 0.1. The acoustic power level (L_W) can be defined as

$$L_{\mathrm{W}} = 10\log(\frac{P_A}{P_{ref}}) \tag{13}$$

where P_{ref} is the reference acoustic power ($P_{ref} = 10^{-12} W/m^2$).

Fig. 10 shows the contour of L_W for scheme 1 and scheme 9. At the trailing edge of the vane suction side, concentrated contour lines can be found. In scheme 9, the distribution of lines is more complex, which is caused by the severe turbulent flow on the suction side. Although there is not any large scale vortex motion in scheme 1, the boundary layer is very thick on the suction side, resulting in the vortex shedding and making contour lines of the acoustic power level more complicated. The values of L_W at most parts in scheme 9 are lower than in scheme 1.

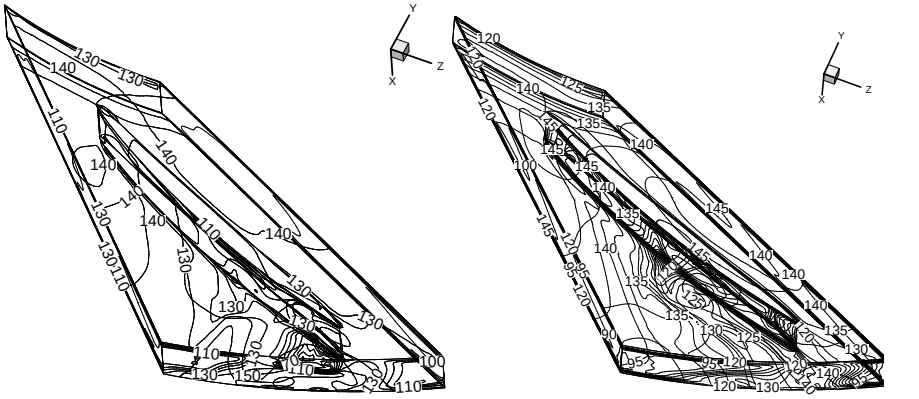

(a) Scheme 1 (b) Scheme 9

Fig.10 Distribution of L_W in diffusers (unit : dB)

The noise source characteristics of the two schemes cannot be distinctly compared through the general distribution of the contour lines of L_W. So, L_W of the two schemes is circumferentially averaged on the sections in the radial direction as is shown in Fig.11, there are 20 cross sections equispaced in the radial direction, L_W is calculated from weighted averages on selected sections. The fluctuation of L_W in scheme 9 is very small on the sections in the radial direction,

about 103~115dB, while in scheme 1 it changes greatly, whose amplitudes are even larger at the trailing edge and the diffuser exit. L_W at diffuser exit and inlet in scheme 1 are higher than in scheme 9. As shown in Fig.6, a supersonic Mach number can be seen at the vane leading edge, the vanes are impacted by the airflow, in conjunction with intense turbulent flow, which lead to the situation that the pressure is too high on the pressure side and too lower on the suction side. The vortex motion in large range at vane trailing edge can cause a high level acoustic power source. The thick boundary layer sheds from the vane surface and results in intense turbulence and high acoustic power level, consequently, L_W in scheme 9 are higher than in scheme 1 at the radius within 0.185~0.23m.

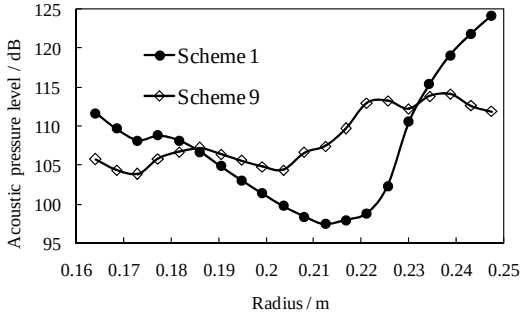

Fig.11 Distribution of L_W along radial direction in diffusers

After being volume-averaged in the computational domain, the values of L_W can be obtained in the whole domain and in each part. In scheme 1, L_W is 112.11dB, while 110.75dB in scheme 9. Therefore, in term of the acoustic performance, the scheme 9 is better than scheme 1.

4. Conclusion

To compare how different design parameters of the diffuser influence its aerodynamic performance and flow noise characteristics, numerical simulation of a centrifugal compressor with a vaned diffuser was carried out. Results show that scheme 9 has a much better performance than scheme 1:

(1)The total pressure decreases gradually in the radial direction in diffuser, and the head loss reaches its maximum at the diffuser exit. The explosive growth of the head losses near the vane leading edge results from the impact between the vanes and the airflow, meanwhile the total pressure descends abruptly.

(2)The supersonic region appears at the diffuser inlet, and an unaccommodated inlet angle of vanes would lead to the vortex motion in large range on the suction side. Therefore, the radius of the round head of the vane leading edge should be minimized to reduce the head losses.

(3)The static pressure recovery coefficient (C_p) and the total pressure loss coefficient (φ) increase gradually in the radial direction. With the development of the flow, the velocity decreases and the energy is converted into static pressure, whose tendency is contrary to the velocity.

(4)The shedding of thick boundary layer and the vortex motion are the main reasons for the high level noise. A proper reduction of the round head radius of vane leading edge can weaken the impact strength of airflow, an appropriate increase of the setting angle of vanes is helpful to lessen the vortex motion at diffuser exit, and the aerodynamic noise level can also be reduced.

REFERENCES

[1] *Kim S, Park J, Ahn K, et al.* "Numerical investigation and validation of the optimization of a centrifugal compressor using a response surface method", Proceedings of the Institution of Mechanical Engineers, Part A: Journal of Power and Energy, **vol.**224(2),2010,pp.251-259..

[2] *LI Du ,YANG Ce, et al.* "Numerical Study of Flow Field of Volute in a Turbocharger Centrifugal Compressor",Transactions of CSICE, **vol.**28(3), 2010,pp.253-259.

[3] *Sun H, Lee S.* "Numerical prediction of centrifugal compressor noise", Journal of sound and vibration, **vol.** 269(1) ,2004,pp. 421-430.

[4] *TAN Wei, QI Ming-xu, LIN Tong, et al.* "Steady on Stability Extension Using Pre-Swirl and Variable Diffuser for Centrifugal Compressor",Chinese Internal Combustion Engine Engineering, **vol.**35(1) ,2014,pp. 69-74.

[5] *DU Jian-Yi, LI Xue-Song, CHU Lei-Zhe, et al.* "Investigation analysis on vaned dissuser",Journal of engineering thermophysics, **vol.**26(1) ,2005,pp.43-46.

[6] *Engeda A.* "Experimental and numerical investigation of the performance of a 240 kW centrifugal compressor with different diffusers", Experimental thermal and fluid Science, **vol.**28(1) ,2003,pp.55-72.

[7] *Sun H, Shin H, Lee S.* "Analysis and optimization of aerodynamic noise in a centrifugal compressor", Journal of sound and vibration, **vol.**289(4) ,2006,pp. 999-1018.

[8] *Ohta Y, Okutsu Y, Goto T, et al.* "Aerodynamic performance and noise characteristics of a centrifugal compressor with modified vaned diffusers", Journal of Thermal Science, **vol.**15(4) ,2006,pp. 289-295.

[9] *Wen H B, Xu W J, Bao S N, et al.* "Experimental research on noise characteristics and mechanism of marine diesel engine turbocharger", Chinese Internal Combustion Engine Engineering, **vol.**34(001) ,2013,pp. 76-80.

[10] *ZHU Da-xin.* "Turbo-charging and Turbocharger", China Machine Press, Beijing,1992.

[11] *K. Jiao et al.,* "Numerical simulation of air flow through turbocharger compressors with dual volute design", Appl Energy, doi:10.1016/j.apenergy.2009.02.019, 2009.

[12] *Tousi, A. M., and A. Tourani.* "Comparison of turbulence methods in CFD analysis of compressible flows in radial turbomachines", Aircraft Engineering and Aerospace Technology, **vol.**80(6),2008,pp. 657-665.

[13] *Peat K S, Torregrosa A J, Broatch A, et al.* "An investigation into the passive acoustic effect of the turbine in an automotive turbocharger", Journal of sound and vibration, **vol.**295(1), 2006,pp.60-75.

[14] *Tiikoja H, Rämmal H, Abom M, et al.* "Investigations of Automotive Turbocharger Acoustics",SAE International Journal of Engines, **vol.**4(2), 2011,pp.2531-2542.